Bulletin of the Seismological Society of America, Vol. 99, No. 4, pp. 2461–2470, August 2009, doi: 10.1785/0120080364

A Local Magnitude Scale for Southern Italy

by Antonella Bobbio, Maurizio Vassallo, and Gaetano Festa

Abstract A local magnitude scale has been defined for southern Italy, in the area monitored by the recently installed Irpinia Seismic Network. Waveforms recorded from more than 100 events of small magnitude are processed to extract synthetic Wood–Anderson traces. Assuming a general description of peak-displacement scaling with the distance, by means of linear and logarithmic contributions, a global exploration of the parameter space is performed by a grid-search method with the aim of investigating the correlation between the two decay contributions and seeking for a physical solution of the problem. Assuming an L^2 norm, we found

$$M = \log A + 1.79 \log R - 0.58,$$

yielding an error on the single estimation smaller than 0.2, at least when the hypocenter location is accurate. Station corrections are investigated through the station residuals, referring to the average value of the magnitude. Using a z test, we found that some stations exhibit a correction term significantly different from 0. The use of the peak acceleration and peak velocity as indicators of the magnitude is also investigated.

Introduction

The local magnitude (M_L) of an earthquake as defined by Richter (1935) is the logarithm of half the peak-to-peak amplitude measured in microns, recorded by a Wood–Anderson seismograph at a distance of 100 km from the epicenter of that earthquake. The Wood–Anderson is a standard torsion seismograph measuring a high-pass filtered displacement with a frequency domain response

$$\mathrm{WA}(f) = -\frac{Vf^2}{(f^2 - \frac{1}{T^2}) + 2ih\frac{f}{T}}, \qquad (1)$$

where f is the frequency, T is the eigenperiod, h is the damping factor that is the ratio between the actual and the critical damping coefficient, and V is the magnification. For a standard Wood–Anderson seismograph $T = 0.8$ sec, $h = 0.8$, and $V = 2800$. These parameters warrant uniformity in the worldwide local magnitude estimates and will be used also in this study to include the Wood–Anderson filtering effect in the records. However, it has been observed that a different choice of the parameters h and V ($h = 0.7$ and $V = 2080$) better synthesizes the Wood–Anderson behavior (Uhrammer and Collins, 1990; Uhrammer *et al.*, 1996). With this latter set of parameters, the Wood–Anderson is equivalent to a high-pass two-pole, causal Butterworth filter with corner frequency of 1.25 Hz.

The magnitude estimation requires a projection of the observed amplitudes at the reference distance. Such a projection is generally referred to as magnitude calibration (e.g., Boore, 1989). In this study we calibrate the local magnitude scale for the Irpinia–Basilicata area, an Appenninic region located in southern Italy that experienced several large earthquakes ($M > 6$) in the last century and is currently monitored by the recently installed Irpinia Seismic Network (ISNet). ISNet is a dense network of 27 stations (triangles in Fig. 1) displaced over an area of approximately 100×70 km along the southern Apennines chain (Weber *et al.*, 2007). To ensure a high dynamic recording range, each seismic station is equipped with a strong-motion accelerometer (Guralp CMG-5T) and a short period three-component seismometer (Geotech S13-J with natural period of 1 sec). At five locations the seismometers are replaced by broadband sensors (Nanometrics Trillium with a flat response in the range 0.025–50 Hz). Data acquisition at the seismic stations is performed by the data-logger Osiris-6 produced by Agecodagis Sarl. The loggers send the data via a dedicated Wi-Fi connection in real time to sparse local control centers (LCC) where they are managed by the EarthWorm system (Johnson *et al.*, 1995). The system automatically individuates seismic events and locates the hypocenter from measurements of P-wave first arrivals. The data are then manually revised before storing in the SeismNet Manager, a database managing waveforms and information from the sites of ISNet (Elia *et al.*, 2009).

During the last century the Irpinia–Basilicata region was struck by three events of magnitude larger than 6: the 1930 M 6.7 Irpinia earthquake (Emolo *et al.*, 2004; Pino *et al.*, 2008) the 1962 M 6.2 Irpinia earthquake (Westaway, 1987),

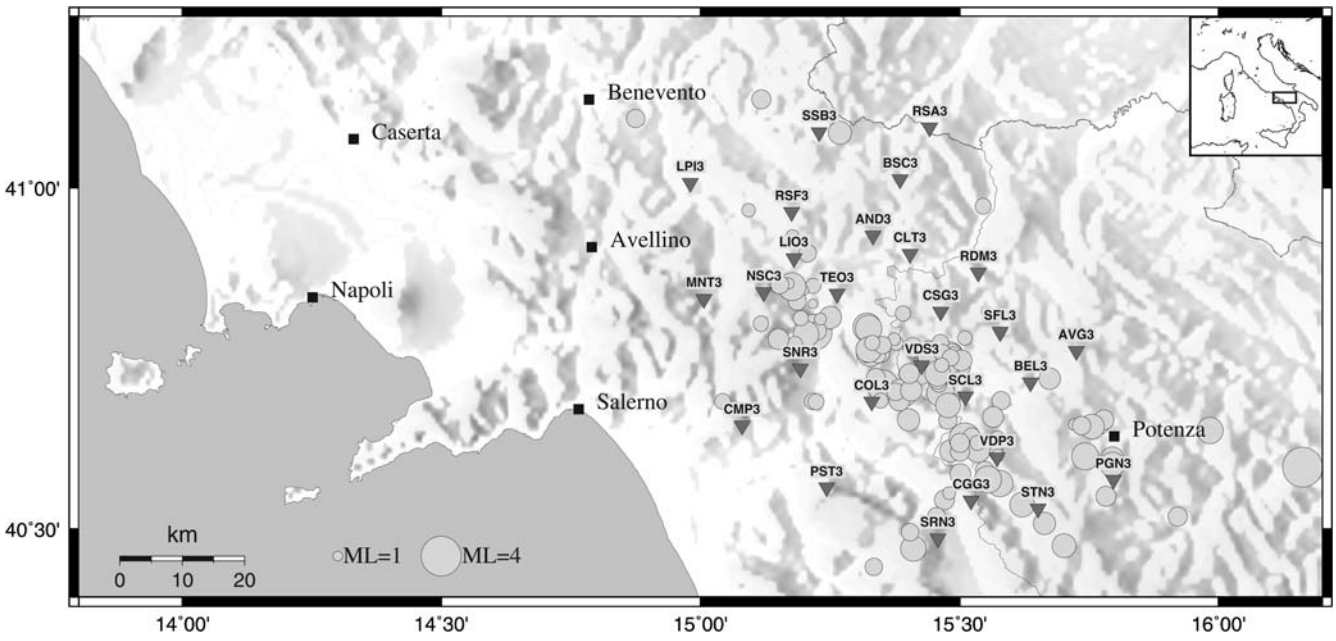

Figure 1. Map of ISNet seismic stations and distribution of earthquakes used in this study. Triangles and circles indicate seismic stations and earthquake locations, respectively.

and the 1980 M 6.9 Irpinia–Basilicata earthquake (Westaway and Jackson, 1987; Bernard and Zollo, 1989; Pantosti and Valensise, 1990). Most of the largest historical events occurred on northwest–southeast oriented normal faults with a few of them having a strike-slip component. The 1980 event, instead occurred on a complex fault system, with at least three main structures activated during the faulting process. Since then, the area has begun to be monitored by the accelerometric network Rete Accelerometrica Nazionale (RAN), held by the National Civil Protection and the broadband Istituto Nazionale di Geofisica e Vulcanologia (INGV) network. During the monitoring period, the regional networks recorded six events of magnitude ranging between 4 and 5.5 and several events of magnitude larger than 3. Since the recent installation of ISNet, the largest events in the region did not exceed magnitude 3.5, with 100 events detected by the network (circles in Fig. 1), mainly located along Appenninic/sub-Appenninic structures that generated the 1980 earthquake. Some are clustered along the right lateral, strike-slip Potenza fault that was responsible for the 1990–1991 sequence, characterized by two main events of magnitude 5.7 and 5.2 and a maximum 7 Mercalli-Cancani-Sieberg (MCS) intensity (Tertulliani *et al.*, 1992). For this reason, the characterization of the size of small events within its location is fundamental to detect space and time variations of the seismicity, as indicators of changes in the tectonic state of the area.

Attenuation of the peak displacement with distance is almost independent of the region for Italy for distances larger than 200 km (Gasperini, 2002), and standard Richter tables can be used to reduce the amplitude at the reference distance. At distances spanned by local networks (5–150 km), anelastic attenuation plays a relevant role in building the high-frequency peak displacement, mostly for small magnitude events where the apparent corner frequency is also driven by scattering and inelastic phenomena. Attenuation laws evaluated for northeastern Italy (Bragato and Tento, 2005); northwestern Alps (Spallarossa *et al.*, 2002; Bindi *et al.*, 2005); and for a few volcanic structures such as Mt. Vesuvius (Del Pezzo and Petrosino, 2001), Mt. Etna (D'Amico and Maiolino, 2005), and the Campi Flegrei area (Petrosino *et al.*, 2008) show significant variations among each other and with the Richter scaling law, raising the need for adaption of M_L scales to the local tectonic setting.

Here we compute a local magnitude scaling relationship for the Irpinia–Basilicata area, using the dataset recorded by ISNet. In the Data section we describe the main features of the data used in this study within the processing required for the computation of the Wood–Anderson peak displacement. In the Local Magnitude Scaling Law section, a global exploration is performed to retrieve the parameters of the attenuation law, which describes the scaling of the peak displacement with the distance. In the following sections, site corrections and comparison with scaling laws from different regions in Italy are discussed. Finally, new parameters, such as peak velocity and peak acceleration, are investigated as indicators for the magnitude evaluation.

Data

In this study a collection of 3000 waveforms recorded by 3-component short period seismometers and accelerometers has been analyzed corresponding to about 100 earthquakes that occurred from September 2005 to June 2008 inside ISNet and in its neighborhood. In Figure 1 ISNet stations are repre-

sented with triangles while epicenters of the events are plotted with circles. To ensure high-quality data, we limit the analysis to traces on which the signal-to-noise ratio is larger than 5 on both the horizontal components. To constrain the magnitude of the event and average out the effects of the distance and azimuth, we additionally require that each event is recorded at least at 4 stations of the network. We finally select the data having a hypocentral distance smaller than 80 km, the value being comparable with the size of the network. The database is not homogeneous in time because it follows the natural deployment and calibration of the instruments. From February to June 2008 ISNet stations recorded a large amount of events of small magnitude ($M < 1.5$) with respect to the past, with the total number of earthquakes comparable to the total recorded during the previous 2.5 yr.

Waveforms are directly downloaded by the SeismNet Manager PostgreSQL database and are available in SAC format along with information about the recording instrument and event location. For each seismic station of ISNet, we analyzed the waveforms recorded by both sensors. After removal of mean value and linear trend, traces are tapered in the time domain with the aim of reducing spurious oscillations in the frequency domain without changing the shape of the signal which is used in the analysis. Data are deconvolved by the instrument response, as reported by the factory calibration chart, integrated in the frequency domain and finally convolved by the Wood–Anderson response (equation 1) before back-transformation in time domain.

The final peak-to peak value to be used for the magnitude estimation has been computed by the algebraic mean of the peak-displacement values measured on both the horizontal components. No significant difference is generally observed between Wood–Anderson displacement peaks coming from velocimeters and accelerometers. In the rare case in which the two measures provide contrasting values, and there is no evidence of malfunctioning of one of the transducers, the datum of that station is discarded.

Local Magnitude Scaling Law

According to the Richter definition, the local magnitude is the log of the peak-displacement A, measured by a Wood–Anderson seismograph, related to a reference amplitude A_0;

$$M = \log A - \log A_0, \tag{2}$$

where the contribution $\log A_0$ accounts for the decay of the peak amplitude with the distance. The Richter scale is calibrated assuming that the magnitude of an event recorded at an epicentral distance of 100 km will be 3 if the maximum amplitude on the Wood–Anderson displacement is 1 mm. Therefore, if the amplitude is measured in millimeters, equation (2) yields $\log A_0(R = 100 \text{ km}) = -3$. As it is frequent practice, we replace the epicentral distance with the hypocentral one in the evaluation of the magnitude (Bragato and Trento, 2005). Because the depth of the earthquakes in this area is at most 20 km, the maximum error on the magnitude estimation is about 1% when assuming 100 km as the hypocentral distance instead of the epicentral distance. This error, albeit systematic, is significantly lower than the error on hypocenter location and on the magnitude estimation coming from the variability in the peak-displacement measurements.

We assume the following functional shape to describe the decay of A_0 with the distance

$$\log A_0 = \alpha \log R + kR + \beta, \tag{3}$$

where the logarithmic term accounts for geometrical spreading, while the linear contribution refers to the anelastic attenuation. The magnitude calibration constrains the value of the constant term to $\beta = -\alpha \log \hat{R} - k\hat{R} - 3$ where $\hat{R} = 100$ km is the reference distance.

With the scaling contribution (3), the attenuation law of the peak displacement (2) can be written as

$$\log A = M + \alpha \log R + kR + \beta. \tag{4}$$

Equation (4) is calibrated on the selected set of events, for each of which we measured the peak-displacement A_{ij} at a limited number of stations located at hypocentral distance R_{ij}

$$\log A_{ij} = M_i + \alpha \log R_{ij} + kR_{ij} + \beta, \tag{5}$$

where the indices i and j are associated with the i-th event and the j-th station, respectively. We estimate the values of the unknowns (M_i, α, k) through the minimization of the L^2 distance between the observed A^{obs} peak displacement and the A^{teo} predicted by the attenuation law

$$\begin{aligned}\Omega(\alpha, k, M_i) &= \frac{1}{n-1}\sum_{i=1}^{n}\sum_{j=1}^{v(i)}(\log A_{ij}^{\text{obs}} - \log A_{ij}^{\text{teo}})^2 \\ &= \frac{1}{n-1}\sum_{i=1}^{n}\sum_{j=1}^{v(i)}(\log A_{ij}^{\text{obs}} - M_i - \alpha \log R_{ij} \\ &\quad - kR_{ij} - \beta)^2\end{aligned} \tag{6}$$

with n, the number of events, and $v(i)$ is the number of stations for which a measure of A is available for the i-th event. The inverse problem consists of finding the best-fit curves for each event, imposing that the scaling with the distance is the same for all of the events. We additionally impose the following constraints:

$$\alpha \le 0; \qquad k \le 0 \tag{7}$$

that account for an effective decay of the peak-amplitude with the distance. The least-squares method equates to zero the first derivatives of the positive-defined function Ω with respect to the parameters but has to arrest on the boundary of the physical domain when the algorithm tries to push the solution in a forbidden region (either $\alpha > 0$ or $k > 0$). Instead of searching a

generalized solution of the least-squares problem, we adopt a two-stage strategy.

For each fixed value of the couple (α, k), we solve n unconnected standard least-squares best-fit problems

$$\chi_i = \sum_{j=1}^{v(i)} (\log A_{ij}^{\text{obs}} - \alpha \log R_{ij} - kR_{ij} - M_i - \beta)^2 \qquad (8)$$

to find the level of the curves $\hat{M}_i(\alpha, k)$ for each single event. This value would represent the magnitude of that event if the values of α and k best describe the decay of the peak with amplitude. Hence, systematically exploring the parameter space spanned by the variables (α, k) we furnish the global minimum solution for the problem by direct computation of the two-dimensional function $\Omega_2(\alpha, k) = \Omega(\alpha, k, \hat{M}_i(\alpha, k))$. Because analytical geometrical spreading predicts a coefficient $\alpha = -1$ for the decay of the direct S wave and $\alpha = -0.5$ for the decay of the nondispersive surface wave, we limit the exploration of the parameter α to the range $-4 \leq \alpha \leq 0$. The variable k ranges between -0.004 and 0, the interval being comparable with the values found elsewhere in Italy (Bragato and Trento, 2005).

In Figure 2 we draw a contour plot of the function $\Omega_2(\alpha, k)$ limited in a subset of the total exploration domain. Tilted ellipses indicate that the parameters α and k are not independent of each other but are correlated along the straight line

$$k = -0.018(\alpha + 1.79). \qquad (9)$$

This valley, which individuates the minimum of one parameter when the other one is fixed, drops down toward the positive k axis and the global minimum falls on the boundary of the investigated domain

$$\alpha = -1.79; \qquad k = 0. \qquad (10)$$

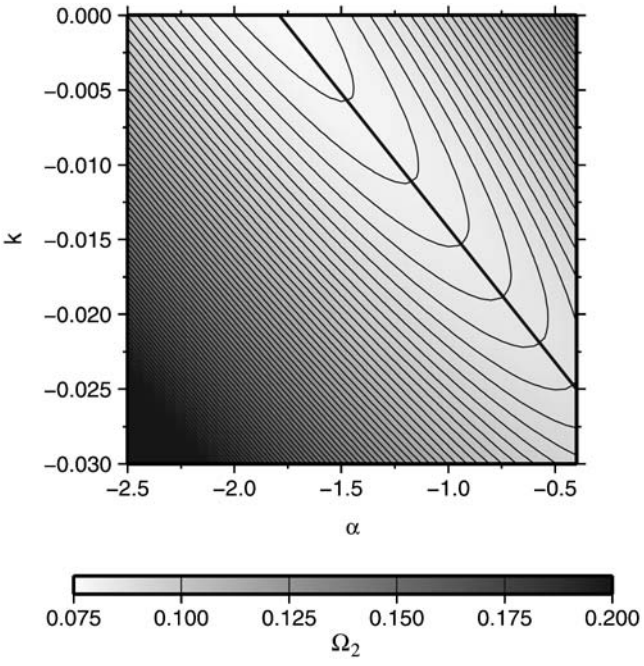

Figure 2. Contour plot of the function Ω_2 as a function of the variables α and k. The stretched ellipses indicate a correlation between the two parameters (the correlation curve is represented by a solid line) with the minimum falling along the α axis.

The isolines in Figure 2 appear to be cut in half by the α axis, indicating that if we had extended the investigation domain in the positive k plane, a lower level of the Ω_2 function would have been encountered there. This solution would be sought out by the standard least-squares technique applied to the function Ω in the domain R^{n+2}.

Our data are therefore modeled with an anelastic coefficient $k = 0$, indicating that in the range of hypocentral distances at which we record the seismic event the anelastic behavior can be included in the logarithmic decay with the distance. This latter has a coefficient $\alpha = -1.79$ that is almost twice the value expected from the analytical decay of the body waves. Therefore, it includes additional effects from wave dispersion and attenuation with respect to simple geometrical spreading. Analogous decay has been found in Japan, and a similar relationship is commonly used for the computation of the local M_{JMA} magnitude in that area (Tsuboi, 1954; Katsumata, 2004).

The error on the parameter α has been estimated by evaluating the width of the Gaussian function

$$e^{-\Omega(\alpha,k,M_i)}|_{k=0;M_i=\hat{M}_i(-1.79,0)} \qquad (11)$$

along the α axis, in correspondence of the minimum of the Ω function, where the other parameters are fixed to the optimal value. We found the error to be 0.03.

Substituting the values of α and k in equation (4), the attenuation law, which better justifies the decreasing of the high-frequency peak displacement with distance, becomes

$$\log A = M - 1.79(\pm 0.03) \log R + 0.58(\pm 0.06). \qquad (12)$$

In Figure 3 we plot $\log(A) - M$ as a function of the hypocentral distance for each record. We also draw the best-fit line (equation 12) through the points with a solid gray line. To check that no dependence on the distance still persists at the boundaries of the investigated range beyond the logarithmic decay, we plot in Figure 4 the residuals, that is, the difference between each data point and the best-fit line as a function of $\log R$. We found that the distribution of the points around the zero level does not change with the distance. Moreover, the cumulative distribution, integrated over the distance, is a Gaussian peaked at zero, strengthening the consistency of our modelling.

Relationship (12) yields an explicit dependence of the magnitude as a function of the peak displacement and the distance

$$M = \log A + 1.79 \log R - 0.58, \qquad (13)$$

allowing for a direct computation of the magnitude within a

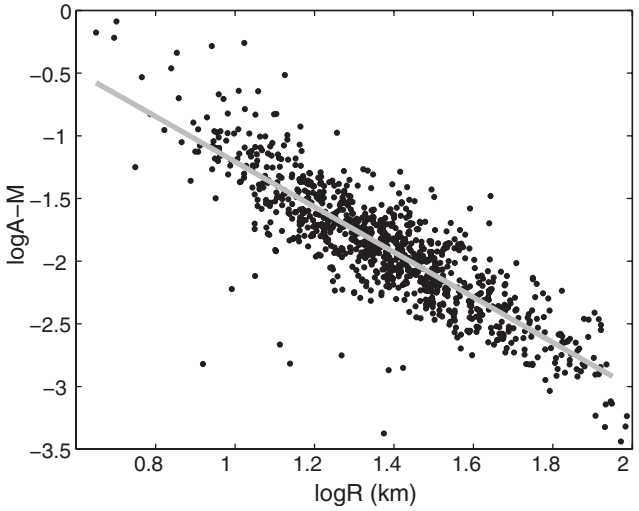

Figure 3. Plot of $\log(A) - M$ as a function of $\log(R)$ for each record. The solid gray line is the best-fit curve of equation (12).

single measure of the peak amplitude. It also provides us with an estimation of the earthquake size when few measures are available. In such a case the projection to 100 km via the least-squares solution becomes ill-conditioned.

The error on the single estimation of the magnitude depends on the errors of the coefficients α and β as well as on the accuracy in the hypocenter location

$$\delta M = \delta\alpha \log R + \alpha \log e \frac{\delta R}{R} + \delta\beta, \tag{14}$$

where e is the Neper number. In Figure 5 we plot δM as a function of the distance for three different values of δR: 3 km (solid line), 1 km (dotted line), and 0.5 km (dashed line), the values being representative of the accuracy on the event location for ISNet. When the location is not accurate (solid line), the error in the magnitude is dominated by the contribution $\frac{\delta R}{R}$, which is as high as 0.5 at short distances from the hypocenter. At larger distances ($R > 60$ km) the influence of

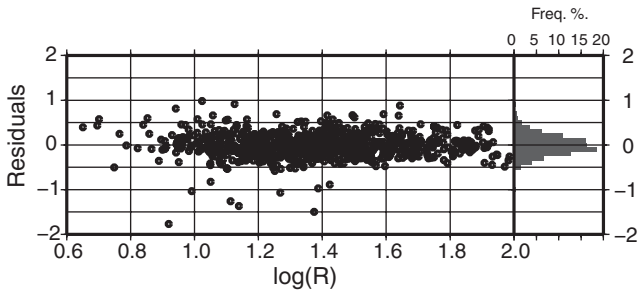

Figure 4. Residuals between the measurements of $\log(A)$ and the best-fit curve (12) as a function of $\log(R)$. No additional effect on the distance beyond the log-decay term is visible at the boundaries of the distance range. Moreover, the data distribution integrated along R has a Gaussian distribution, reinforcing the consistency of our processing.

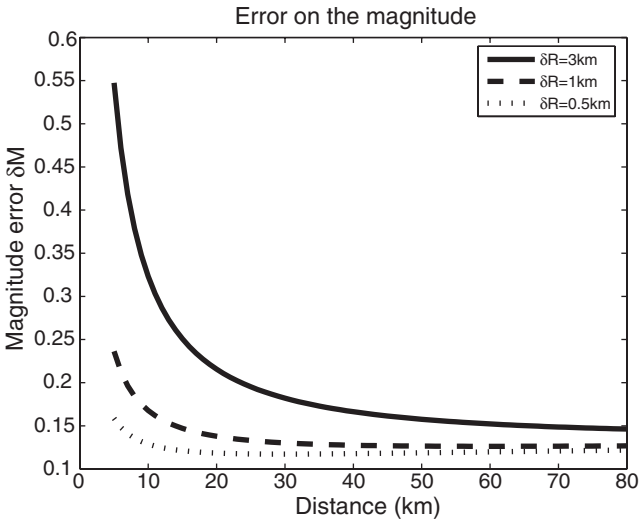

Figure 5. Error in magnitude as a function of the hypocentral distance plotted in a log scale for three different values of the error for the distance $\delta R = 3$ km (solid line), 1 km (dashed line), 0.5 km (dotted line). When the location is inaccurate, the error on the magnitude estimation can be as high as 0.6. In the other cases it drops down to 0.2–0.3 over the whole distance range.

the contribution $\delta\alpha \log R$ becomes comparable with the decay term $\frac{\delta R}{R}$, and the total error on the magnitude decreases below 0.2.

The latter value is also the standard error on the magnitude in the whole distance range when the location of the hypocenter is accurate.

When several stations record the seismic event, each station calculates a single estimation of the magnitude from relationship (13). The magnitude of the event, as defined in the least-squares sense, averages out the peak-displacement measurements over the distance, minimizing the L^2-norm χ of equation (8). Assuming M_j the magnitude value provided by the j-th station, the χ function is

$$\chi = \sum_{j=1}^{v} (\log A_j - M - \alpha \log R_j - \beta)^2 = \sum_{j=1}^{v} (M_j - M)^2, \tag{15}$$

being α and β fixed to the previously found values. Differentiating with respect to M and equating the derivative to zero, we have

$$\sum_{j=1}^{v} (M_j - M) = 0. \tag{16}$$

Hence, the best estimate for the magnitude, in the least-squares sense, is the algebraic mean of the magnitude values measured at all the recording stations.

Comparison with Other Local Magnitude Scales

In Figure 6 we plot the decay of the Wood–Anderson peak displacement with the distance, represented as $\log A_0$ for the Irpinia–Basilicata area (solid black line). For comparison, we also add the values of $\log A_0$ (dashed black line) used for California with the corrections of Hutton and Boore (1987), as well as the decay laws used for the magnitude estimation in northwestern Italy (Bindi *et al.*, 2005; dashed gray line) and northeastern Italy (Bragato and Tento, 2005; dotted gray line). The Hutton and Boore curve is also used by the INGV to build up the official bulletin for Italy (Amato and Mele, 2008) to be used by the national civil protection for emergency planning.

The four curves are not superimposed at all distances but are close to each other only in limited distance ranges. This clearly indicates that inelastic attenuation of waves locally plays a significant role in the definition of strong ground motion parameters and accurate estimates of the quality factor Q are needed for both ground-motion modeling and source properties retrieval. Specifically, the decay of the peak displacement in the Irpinia–Basilicata follows the same trend of the curve for northwestern Italy. At smaller distances (<30 km) we observe a higher level of $\log A_0$ with respect to the other decay laws, indicating a smaller attenuation as compared to other regions in Italy.

The local magnitude computed by the INGV is available for all the events used in this work. This value is computed over Wood–Andserson displacements synthesized by broadband velocimeters installed in the same area with a larger average spacing. In Figure 7 we compare the magnitude computed on the ISNet data with the values furnished by the INGV catalog. Specifically, black points refer to the average magnitude, while gray points indicate the dispersion of the single measures around the average value.

The solid line represents the best-fit curve defining the relationship between the local magnitude computed with data from the two networks

$$M_{\mathrm{ISNet}} = 0.92 M_{\mathrm{INGV}} + 0.28. \qquad (17)$$

Such a relationship should be compared to the bisector, plotted with a dashed line. We find a discrepancy between the two laws, mostly between $0.5 < M < 1$, as high as 0.24 units. The difference decreases as the magnitude increases and drops down to 0.04 for M 3.0.

Station Corrections

The magnitude estimation provided by the j-th station M_{ij} is not expected to be coincident with the average value M_i because of variability in the source and path properties or instrument installation (Richter, 1958). Let us define the station correction coefficient $S_j = m(M_{ij} - M_i)$ as the mean value of the distribution of the residuals over a large set of events. We expect that $S_j = 0$. When it is no longer true, local amplification associated with shallow layering influences the low-frequency amplitudes of the signal. A positive/negative mean value will correspond to an amplification/deamplification of seismic waves at the site so that the distribution of station correction coefficients describes the general site conditions in the study area.

We estimate the static correction at each ISNet site S_j with the restriction that at least five stations have contributed to the mean value M_i of each event. For the analysis, we assume a Gaussian distribution of the residuals, parametrized through the mean and the standard error of the mean. Figure 8

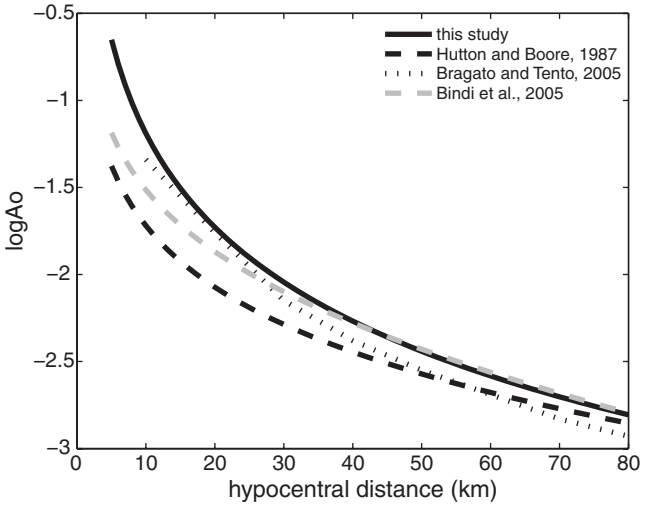

Figure 6. Plot of $\log A_0$ as a function of the hypocentral distance for the Irpinia–Basilicata area (solid black line), northwestern Italy (dashed gray line) and northeastern Italy (dotted gray line). All curves are compared to the Richter decay table with the corrections of Hutton and Boore (1987) represented here with a dashed black line.

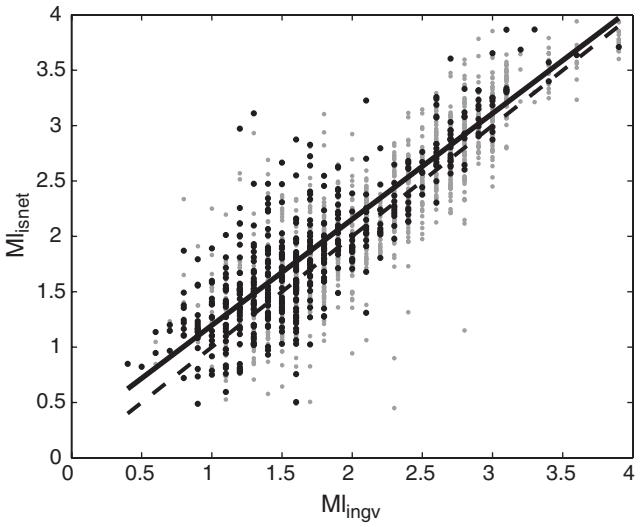

Figure 7. Comparison between the local magnitude computed using the ISNet data and the catalog value in the INGV bulletin. Black points refer to the average M_{L} value computed on the ISNet data for each single event, while gray points are associated with the single station magnitude estimation.

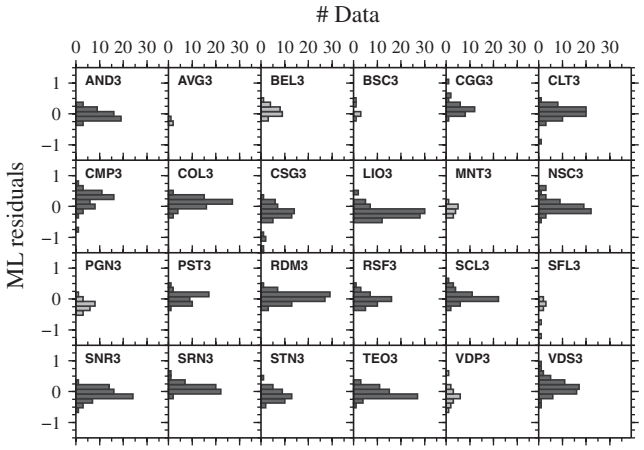

Figure 8. Histograms of M_L residuals for all the stations of ISNet. Magnitude data are binned in intervals of width 0.15. Light gray histograms are stations for which less than 30 observations are available.

shows the frequency of residuals binned in intervals of 0.15. In Table 1 the parameters of the Gaussian distribution for each station are summarized.

Several stations (AVG3, BEL3, BSC3, MNT3, PGN3, SFL3, VDP3) do not have a sample large enough ($N > 30$) to warrant the correct reconstruction of the Gaussian shape of distribution and are not used for the analysis. This choice also avoids large station corrections that can occur when only few earthquakes are recorded (Miao and Langston, 2007). All the remaining distributions show a Gaussian-like shape with mean values included into the range [−0.25; 0.24] and standard deviations into the range (0.13; 0.36). The relatively high values of standard deviation observed for several stations

Table 1

Parameters of the Gaussian Distribution of the Residuals for Stations of the ISNet Network*

Station	Mean	σ_m	σ	z	N° Data
AND3	**−0.03**	0.02	**0.15**	**−0.64**	**50**
CGG3	**0.19**	**0.04**	**0.21**	**2.94**	**31**
CLT3	0.05	0.03	0.20	1.09	63
CMP3	**0.24**	**0.04**	**0.27**	**4.25**	**50**
COL3	**0.12**	**0.02**	**0.16**	**2.88**	**66**
CSG3	**-0.25**	**0.05**	**0.35**	**−3.86**	**51**
LIO3	**-0.20**	**0.03**	**0.18**	**−5.16**	**84**
NSC3	0.00	0.03	0.20	−0.06	61
PST3	0.04	0.02	0.15	0.74	40
RDM3	0.05	0.02	0.15	1.27	80
RSF3	−0.02	0.02	0.17	−0.45	42
SCL3	0.07	0.02	0.18	1.42	49
SNR3	−0.08	0.03	0.18	−1.77	66
SRN3	**0.11**	**0.03**	**0.13**	**2.44**	**53**
STN3	**−0.11**	**0.02**	**0.20**	**−2.01**	**40**
TEO3	−0.05	0.03	0.16	−1.13	61
VDS3	**0.15**	**0.03**	**0.24**	**3.06**	**61**

*The z score is the statistical parameter used to test the hypothesis that the observed residuals distribution has zero mean. The stations in bold are those for which an S_j value different from zero is observed.

(CMP3, LIO3, CSG3, SCL3, SNR3, VDS3) can be explained as the effects of regional scale wave propagation and seismic source effects such as focal mechanism that are not accounted for into the definition of M_L.

A statistical z test has been performed to evaluate whether the computed S_j is significantly different from zero. Specifically, we test the hypothesis that the observed residuals distribution coincides with the theoretical distribution with zero mean and a standard deviation of 0.3, the latter value being representative of the error on the magnitude. We defined for the j-th station the variable z_j

$$z_j = \frac{S_j}{\sqrt{\frac{\sigma_j^2 - \sigma_T^2}{N_j}}}, \tag{18}$$

where $\sigma_T = 0.3$, and N_j is the sample dimension for the j-th station. The z-score, reported in Table 1, is the difference of the mean values over the difference between the standard deviations associated with the mean. The stations with $|z_j| > 1.96$ (CGG3, CMP3, COL3, CSG3, LIO3, SRN3, STN3, VDS3) have mean values different from zero with a significance level of 5%. For the remaining stations there is no evidence for rejecting the null hypothesis.

Peak-Velocity and Peak-Acceleration Scaling Law

Local magnitude is linked to the Wood–Anderson peak displacement that has been synthesized from integration of velocity or acceleration data. Nevertheless, direct measures of peak velocity or peak acceleration for small magnitude events can be informative of their size. Using the same dataset over which we estimated the magnitude from peak-displacement observations, we investigate the correlation between the magnitude and the peak velocity/peak acceleration measured on the whole trace. For the analysis, data have been filtered in the frequency band 1.25–25 Hz. It allows the broadband signals to be directly compared with the short period data while we guarantee that acceleration data have a high signal-to-noise ratio also for small magnitude events ($M \leq 1$).

For the general peak measurement PGX (equals Peak Ground Velocity [PGV] or Peak Ground Acceleration [PGA]), we seek a relationship

$$M = a \log \mathrm{PGX} + b \log R + c, \tag{19}$$

which allows for the computation of the magnitude when the hypocentral distance is known. Through a best-fit analysis we achieved the following relationships:

$$\begin{aligned} M_{\mathrm{PGV}} &= 0.770(\pm 0.017) \log \mathrm{PGV} + 1.70(\pm 0.04) \log R \\ &\quad + 3.48(\pm 0.08) \\ M_{\mathrm{PGA}} &= 0.67(\pm 0.02) \log \mathrm{PGA} + 1.75(\pm 0.06) \log R \\ &\quad + 1.82(\pm 0.08), \end{aligned} \tag{20}$$

where velocity is measured in m/sec and acceleration in m/sec^2. We remark that the dependence on distance remains almost unchanged, while the coefficient of the peak scaling decreases as we move from displacement to acceleration indicating that information on coherent average source properties is lost when moving toward the high-frequency range. In Figure 9 we plot the residual of the best-fit lines for the peak velocity (top panel) and peak acceleration (bottom panel) as a function of the distance. Residuals are stacked in the cumulative histograms on the right sides of the panels.

Although the residuals are concentrated around zero, dispersion of the data is significantly larger for acceleration measurements with a standard error on average of 0.5. Again, there is no significant dependence on the distance. To quantitatively assess the uncertainties on the magnitude, we propagate the errors on the single parameters, as well as on the hypocentral distance. Generalization of formula (14) yields

$$\delta M = \delta a \log \mathrm{PGX} + \delta b \log R + b \log e \frac{\delta R}{R} + \delta c, \quad (21)$$

which now depends on the specific value of log PGX. In Figure 10 we plot the error on the magnitude achieved for peak displacement, peak velocity, and peak acceleration. The two classes of curves refer to two values of hypocenter location error ($\delta r = 0.5$ km and $\delta r = 3$ km) that are representative of the accuracy of the location in ISNet as discussed in the Local Magnitude Scaling Law section. For each class, the curve refer to the peak displacement (solid thick line) is independent of the magnitude by definition. The error on the magnitude for peak velocity and peak acceleration depends on the peak value that provided such a magnitude instead as shown in formula (20).

Dashed and dotted lines refer to the error associated with the PGV and PGA, respectively, the lower curve being drawn in correspondence is for M 1 and the upper for M 3. In any case, we see that at large distances ($R > 40$ km) the error on the magnitude from PGV and PGA is significantly larger than the error related to the peak displacement. At these distances the two classes of curves tend to an average value ranging between 0.25 and 0.35. Such an error is comparable with the error associated with the final value of magnitude averaged over several azimuthally distributed stations. Finally, the error related to the PGA is slightly larger than the one related to the PGV.

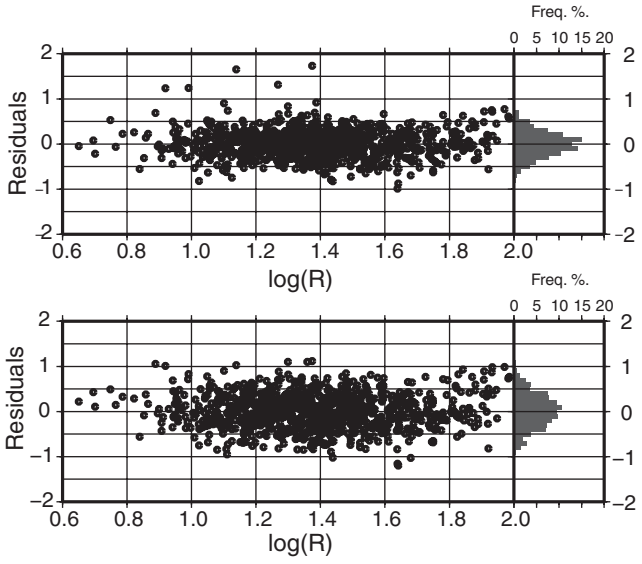

Figure 9. Magnitude residuals from peak velocity (top panel) and peak acceleration (bottom panel) measurements as a function of the distance, along with histograms representing the residual distribution integrated along the distance. Peak-acceleration data exhibit a larger dispersion as compared to peak-velocity measurements.

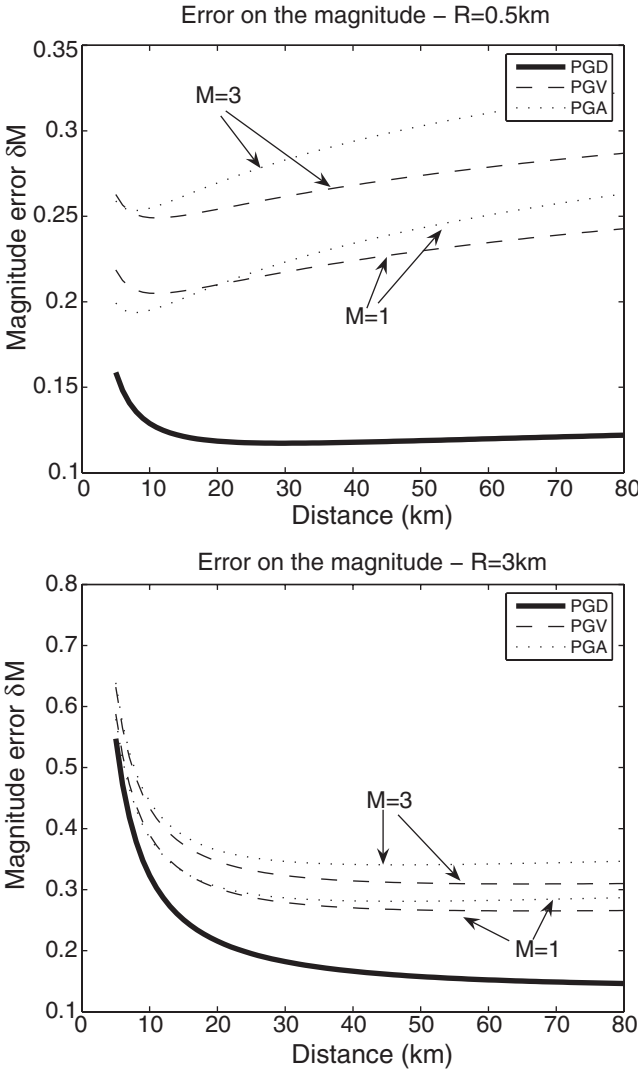

Figure 10. Magnitude error curves as function of the distance for two values of the error on the hypocentral distance $\delta r = 0.5$ km (top panel) and $\delta r = 3$ km (bottom panel). In each figure, the solid line refers to the error associated with the peak displacement, the dashed lines to the peak velocity, and the dotted lines to the peak acceleration. In each panel, two curves are drawn for peak velocity and peak acceleration associated with magnitude M 1 and M 3, respectively.

Conclusions

In this study, a local magnitude scale has been calibrated for southern Italy, in the area struck by the 1980 Irpinia earthquake where a dense seismic network (ISNet) has been installed for early warning purposes. In view of a large event ($M > 5.5$), the occurrence probability of which has been estimated to be 25% in the next 10 yr (Cinti *et al.*, 2004), ISNet is also aimed at monitoring the level of seismicity in the area and possibly detecting variations in the local state of the stress. As a consequence the macroscopic characterization of the seismic source plays a key role, and ad hoc magnitude scales are required to investigate the details of small earthquakes rupture processes.

We processed waveforms from about 100 earthquakes to extract synthetic Wood–Anderson displacements over which the measure of peak amplitude has been performed. Assuming a decay with distance according to equation (3), we performed a global exploration of the decay contributions with a two-step procedure. For any fixed value of the decay coefficients (α, k), we computed the magnitude of all the events by solving n unconnected linear problems. Therefore, we chose as a solution the couple that minimizes the distance between observed and predicted amplitudes in the least-squares sense. This technique allowed for the investigation of the correlation between α and k, as well as for accounting for the constraints on the sign of both parameters.

We found the best solution to be $\alpha = 1.79$ and $k = 0$. The error associated with the magnitude estimate from the single station can be as small as 0.1 when the hypocenter location is accurate (location error smaller than 1 km). However, when averaging the magnitude at different stations we found a standard deviation of about 0.3.

When comparing the scaling with distance found in this work to other scaling laws, we found significant differences, mostly concentrated at short distances ($R < 30$ km). As concerns the magnitude, comparison with INGV estimations on a common dataset shows that the national bulletin underestimates the magnitude for events occurred in the Irpinia–Basilicata area in the range $0.5 < M < 3$ with discrepancies of 0.24 at the lower limit of the exploration interval.

We investigated static station corrections through the mean of the distribution of the residuals, that is, the difference between the magnitude provided by that station and the average magnitude. A statistical test has been performed to evaluate how significant from 0 such a mean value is. With a significance level of 5%, we found that for eight stations (CGG3, CMP3, COL3, CSG3, LIO3, SRN3, STN3, VDS3) the correction coefficient is different from 0. We were not able to correlate such coefficients to local site effects, because most stations are located in a Tertiary area. Specific analyses are, therefore, required to investigate the shallow structure below the stations as well as the effect of the topography, which is often very steep in the area.

We finally discussed the possibility of using direct measures of peak velocity and peak acceleration for the estimation of the magnitude. To evaluate the goodness of the indicator, we propagated the error of the linear regression as a function of the distance at which the measure is performed. We found a general degradation of the magnitude estimation when moving to the high-frequency range. Although the estimate provided by the Wood–Anderson displacements is significantly more accurate than both estimations coming from PGV and PGA, the error on the single estimate of the magnitude is comparable to one obtained by the average standard M_L when the hypocenter position is trustworthy.

Data and Resources

Seismic data used in this study were collected by ISNet (Irpinia Seismic Network) managed by Amra Scarl (Analisi e Monitoraggio del Rischio Ambientale) and are available online at http://dbserver.ov.ingv.it:8080 (last accessed May 2009). Data availability is subject to registration. Some of the figures are made with the software Generic Mapping Tools (www.soest.hawaii.edu/gmt, last accessed February 2009).

Acknowledgments

The authors gratefully thank G. Iannaccone and A. Zollo for helpful discussions, the associate editor Cezar Trifu, and two anonymous reviewers for their valuable contribution in improving the manuscript. This research has partially benefited from funding provided by the Italian Presidenza del Consiglio dei Ministri–Dipartimento della Protezione Civile (DPC). Scientific papers funded by DPC do not represent its official opinion and policies.

References

Amato, A., and F. M. Mele (2008). Performance of the INGV National Seismic Network from 1997 to 2007, *Ann. Geophys.* **51,** no. 2/3, 99–113.

Bernard, P., and A. Zollo (1989). The Irpinia (Italy) 1980 earthquake: Detailed analysis of a complex normal faulting, *J. Geophys. Res.* **B94,** 1631–1647.

Bindi, D., D. Spallarossa, C. Eva, and M. Cattaneo (2005). Local and duration magnitudes in northwestern Italy, and seismic moment versus magnitude relationships, *Bull. Seismol. Soc. Am.* **95,** 592–604.

Boore, D. M. (1989). The Richter scale: Its development and use for determining earthquake source parameters, *Tectonophysics* **166,** 1–14.

Bragato, P. L., and A. Tento (2005). Local magnitude in northeastern Italy, *Bull. Seismol. Soc. Am.* **95,** 579–591.

Cinti, F. R., L. Faenza, W. Marzocchi, and P. Montone (2004). Probability map of the next $M \geq 5.5$ earthquakes in Italy, *Geochem. Geophys. Geosyst.* **5,** Q11003, doi 10.1029/2004GC000724.

D'Amico, S., and V. Maiolino (2005). Local magnitude estimate at Mt. Etna, *Ann. Geophys.* **48,** no. 2, 215–229.

Del Pezzo, E., and S. Petrosino (2001). A local magnitude scale for Mt. Vesuvius from synthetic Wood—Anderson seismograms, *J. Seismol.* **5,** 207–215.

Elia, L., C. Satriano, and G. Iannaccone (2008). SeismNet manager—A web application to manage hardware and data of a seismic network, *Seism. Res. Lett.* **80,** no. 3, 420–430.

Emolo, A., G. Iannaccone, A. Zollo, and A. Gorini (2004). Inferences on the source mechanisms of the 1930 Irpinia (southern Italy) earthquake from simulations of the kinematic rupture process, *Ann. Geophys.* **47,** 1743–1754.

Gasperini, P. (2002). Local magnitude revaluation for recent Italian earthquakes (1981–1996), *J. Seismol.* **6,** 503–524.

Hutton, L. K., and M. Boore (1987). The M_L scale in southern California, *Bull. Seismol. Soc. Am.* **77,** 2074–2094.

Johnson, C. E., A. Bittenbinder, B. Bogaert, L. Dietz, and W. Kohler (1995). Earthworm: A flexible approach to seismic network processing, *IRIS Newsletter* **14,** no. 2, 1–4.

Katsumata, A. (2004). Revision of the JMA displacement magnitude, *Quart. J. Seis.* **67,** 1–10.

Miao, Q., and C. A. Langston (2007). Empirical distance and the local-magnitude scale for the central United States, *Bull. Seismol. Soc. Am.* **97,** 2137–2151.

Pantosti, D., and G. Valensise (1990). Faulting mechanism and complexity of the 23 November 1980, Campania-Lucania earthquake, inferred from surface observations, *J. Geophys. Res.* **95,** 15319–15341.

Petrosino, S., L. De Siena, and E. Del Pezzo (2008). Re-calibration of the magnitude scales at Campi Flegrei, Italy, on the basis of measured path and site and transfer functions, *Bull. Seismol. Soc. Am.* **98,** 1964–1974.

Pino, A. N., B. Palombo, G. Ventura, B. Perniola, and G. Ferrari (2008). Waveform modeling of historical seismograms of the 1930 Irpinia earthquake provides insight on "blind" faulting in southern Apennines (Italy), *J. Geophys. Res.* **113,** B05303.

Richter, C. F. (1935). An instrumental earthquake magnitude scale, *Bull. Seismol. Soc. Am.* **25,** 1–32.

Richter, C. F. (1958). *Elementary Seismology*, W. H. Freeman and Co., San Francisco, California, 768 pp.

Spallarossa, D., D. Bindi, P. Augliera, and M. Cattaneo (2002). An M_L scale in northwestern Italy, *Bull. Seismol. Soc. Am.* **92,** 2205–2216.

Tertulliani, A., M. Anzidei, A. Maramai, M. Murru, and F. Riguzzi (1992). Macroseismic study of the Potenza (southern Italy) earthquake of 5 May 1990, *Nat. Hazards* **6,** 25–38.

Tsuboi, C. (1954). Determination of the Gutenberg-Richter's magnitude of shallow earthquakes occurring in and near Japan (in Japanese), *Zisin* **7,** 185–193.

Uhrammer, R. A., and E. R. Collins (1990). Synthesis of Wood–Anderson seismograms from broadband digital records, *Bull. Seismol. Soc. Am.* **80,** 702–716.

Uhrhammer, R. A., S. Loper, and B. Romanowicz (1996). Determination of local magnitude using BDSN broadband records, *Bull. Seismol. Soc. Am.* **86,** 1314–1330.

Weber, E., V. Convertito, G. Iannaccone, A. Zollo, A. Bobbio, L. Cantore, M. Corciulo, M. Di Crosta, L. Elia, C. Martino, A. Romeo, and C. Satriano (2007). An advanced seismic network in the southern Apennines (Italy) for seismicity investigations and experimentation with earthquake early warning, *Seism. Res. Lett.* **78,** 622–534.

Westaway, R. (1987). The Campania, southern Italy, earthquakes of 1962 August 21, *Geophys. J. R. Astr. Soc.* **8,** 1–24.

Westaway, R., and J. Jackson (1987). The earthquake of 1980 November 23 in Campania-Basilicata (southern Italy), *Geophys. J. R. Astr. Soc.* **90,** 375–443.

Istituto Nazionale di Geofisica e Vulcanologia
Osservatorio Vesuviano
via Diocleziano 328
80124 Napoli, Italy
(A.B.)

Analisi e Monitoraggio Ambientale (AMRA) Scarl
via Nuova Agnano 11
80124 Napoli, Italy
(M.V.)

Dipartimento di Scienze Fisiche
Università di Napoli Federico II
Complesso Universitario Monte S. Angelo
via Cinthia
80124 Napoli, Italy
(G.F.)

Manuscript received 12 December 2008